Surface emitting terahertz quantum cascade laser with a double-metal waveguide

Jonathan A. Fan, Mikhail A. Belkin, and Federico Capasso

Division of Engineering and Applied Sciences, Harvard University, Cambridge, MA 02138
capasso@deas.harvard.edu

Suraj Khanna, Mohamed Lachab, A. Giles Davies, and Edmund H. Linfield

School of Electronic and Electrical Engineering, University of Leeds, Leeds LS2 9JT, UK

Abstract: We investigate the implementation of surface emission via a second order grating in terahertz quantum cascade lasers with double-metal waveguides. Absorbing edge structures are designed to enforce anti-reflecting boundary conditions, which ensure distributed feedback in the cavity. The grating duty cycle is chosen in order to maximize slope efficiency. Fabricated devices demonstrate surface emission output powers that are comparable to those measured from edge-emitting double metal waveguide structures without gratings. The slope efficiency of surface emitting lasers is twice that of double-metal edge emitting structures. Surface emitting lasers show single mode behavior, with a beam divergence along the laser ridge of approximately six degrees.

OCIS codes: (140.3070) Infrared and far-infrared lasers; (140.3490) Lasers, distributed-feedback; (250.7270) Vertical emitting lasers; (130.0250) Optoelectronics

References and links

1. R. Köhler, A. Tredicucci, F. Beltram, H. E. Beere, E. H. Linfield, A. G. Davies, D. A. Ritchie, R. C. Iotti, and F. Rossi, "Terahertz semiconductor-heterostructure laser," Nature **417**, 156 (2002).
2. B. S. Williams, S. Kumar, Q. Hu, and J. L. Reno, "Operation of terahertz quantum-cascade lasers at 164 K in pulsed mode and at 117 K in continuous-wave mode," Opt. Express **13**, 3331 (2005).
3. K. Unterrainer, R. Colombelli, C. Gmachl, F. Capasso, H. Y. Hwang, D. L. Sivco, and A. Y. Cho, "Quantum cascade lasers with double metal-semiconductor waveguide resonators," Appl. Phys. Lett. **80**, 3060 (2002).
4. B. S. Williams, S. Kumar, H. Callebaut, Q. Hu, and J. L. Reno, "Terahertz quantum-cascade laser at λ≈100 μm using metal waveguide for mode confinement," Appl. Phys. Lett. **83**, 2124 (2003).
5. A. J. L. Adam, I. Kasalynas, J. N. Hovenier, T. O. Klaassen, J. R. Gao, E. E. Orlova, B. S. Williams, S. Kumar, Q. Hu, and J. L. Reno, "Beam patterns of terahertz quantum cascade lasers with subwavelength cavity dimensions," Appl. Phys. Lett. **88**, 151105 (2006).
6. S. Kohen, B. S. Williams, and Q. Hu, "Electromagnetic modeling of terahertz quantum cascade laser waveguides and resonators," J. Appl. Phys. **97**, 053106 (2005).
7. D. Hofstetter, J. Faist, M. Beck, and U. Oesterle, "Surface-emitting 10.1 μm quantum-cascade distributed feedback lasers," Appl. Phys. Lett. **75**, 3769 (1999).
8. C. Pflügl, M. Austerer, W. Schrenk, S. Golka, G. Strasser, R. P. Green, L. R. Wilson, J. W. Cockburn, A. B. Krysa, and J. S. Roberts, "Single-mode surface-emitting quantum-cascade lasers," Appl. Phys. Lett. **86**, 211102 (2005).
9. O. Demichel, L. Mahler, T. Losco, C. Mauro, R. Green, J. H. Xu, A. Tredicucci, F. Beltram, H. E. Beere, D. A. Richie, and V. Tamosiunas, "Surface plasmon photonic structures in terahertz quantum cascade lasers," Opt. Express **14**, 5335 (2006).
10. G. Scalari, N. Hoyler, M. Giovannini, and J. Faist, "Terahertz bound-to-continuum quantum-cascade lasers based on optical-phonon scattering extraction," Appl. Phys. Lett. **86**, 181101 (2005).
11. H. Kogelnik and C.V. Shank, "Coupled-wave theory of distributed feedback lasers," J. Appl. Phys. **43**, 2327 (1972).
12. R. F. Kazarinov and C. H. Henry, "Second-order distributed feedback lasers with mode selection provided by first-order radiation losses," IEEE J. Quantum Electron. **QW-21**, 144 (1985).
13. R. J. Noll and S. H. Macomber, "Analysis of grating surface emitting lasers," IEEE J. Quantum Electron. **26**, 456 (1990).
14. N. Finger, W. Schrenk, and E. Gornik, "Analysis of TM-polarized DFB laser structures with metal surface gratings," IEEE J. Quantum Electron. **36**, 780 (2000).

#75601 - $15.00 USD Received 29 September 2006; revised 26 October 2006; accepted 9 November 2006

15. M. Schubert and F. Rana, "Analysis of terahertz surface emitting quantum-cascade lasers," IEEE J. Quantum Electron. **42**, 257 (2006).
16. S. R. Chinn, "Effects of mirror reflectivity in a distributed-feedback laser," IEEE J. Quantum Electron. **QE-9**, 574 (1973).
17. W. Streifer, R. D. Burnham, and D. R. Scifres, "Effect of external reflectors on longitudinal modes of distributed feedback lasers," IEEE J. Quantum Electron. **QE-11**, 154 (1975).
18. S. Barbieri, J. Alton, H. E. Beere, J. Fowler, E. H. Linfield, and D. A. Ritchie, "2.9 THz quantum cascade lasers operating up to 70 K in continuous wave," Appl. Phys. Lett. **85**, 1674 (2004).

1. Introduction

The terahertz (THz) spectral range (1-10 THz) has historically been devoid of a compact source of coherent radiation. There are many applications for coherent THz sources, including medical imaging, security screening, heterodyne receivers, spectroscopy, and trace gas detection. Recently, quantum cascade lasers (QCLs) were developed as a novel source for THz radiation [1] and have rapidly covered the frequency range 2-5 THz. Terahertz QCLs can operate at temperatures as high as 164K [2], and there is strong interest in pushing the operating temperature to a range supported by thermoelectric coolers.

A proper waveguide design is critical to achieve good temperature performance in THz QCLs. The waveguide must provide for low lasing threshold, high slope efficiency, and high mode confinement within the QCL active region, which is typically an order of magnitude thinner than the wavelength of THz radiation in air. Currently, the best temperature performance is achieved with so-called double-metal waveguides, Fig. 1(a) [3]. These waveguides are fabricated using a wafer bonding technique [2-4] and have metal cladding on both sides of the active region. Their structure is essentially the same as that of microstrip transmission lines widely used for waveguiding at microwave frequencies. These waveguides provide low losses due to the shallow skin depth of the TM-polarized QCL mode in the metal, and the mode confinement factor within the QCL active region is near unity.

Most THz QCLs to date are edge emission devices based on Fabry-Perot resonators. As a result of strong mode confinement in a subwavelength-thick active region, the far-field profile in edge-emitting double-metal waveguide THz QCLs is highly non-directional, [5] and slope efficiency is poor [6]. Poor slope efficiency results from strong beam divergence and from mirror losses α_M that are small relative to waveguide losses α_W which makes the outcoupling factor $\alpha_M/(\alpha_{M+}\alpha_W)$ small. One way to increase slope efficiency and avoid the strong beam divergence, while still preserving high mode confinement, is to configure the waveguide for surface emission via a second-order grating in double-metal waveguides. Second-order grating surface emitting devices have already been demonstrated in dielectric waveguides for mid-IR QCLs [7,8]. Very recently, surface emission with a second-order grating has also been demonstrated in THz QCLs with a single-metal waveguide [9].

The single-metal waveguide is an alternative waveguide design for THz QCLs [1]. It uses a metal layer and a highly doped semiconductor layer above and below the active region, respectively [Fig. 1(b)]. These waveguides are easier to process than double-metal waveguides, but they provide only 15-50% of THz mode confinement in the QCL active region [6]. The smaller confinement factor may be a reason why the temperature performance of single-metal waveguide THz QCLs is worse than that of double-metal waveguide devices [10].

The optimal second-order grating designs for surface emission in single- and double-metal THz QCLs are different. For single-metal waveguides, the metal openings cannot be too large because the metal layer is responsible for mode waveguiding; the low-loss surface plasmon mode structure is preserved only if the grating openings support surface plasmon tunneling [9]. In Ref. [9], the grating openings are optimized to be 4% of the total grating period. This may significantly limit the output power and slope efficiency of the device. For double-metal waveguide THz QCLs, low-loss waveguiding is possible with larger grating openings in the top metal cladding. For the surface emitting structures discussed, the optimum opening size is calculated to be ~35% of the total grating period.

#75601 - $15.00 USD Received 29 September 2006; revised 26 October 2006; accepted 9 November 2006

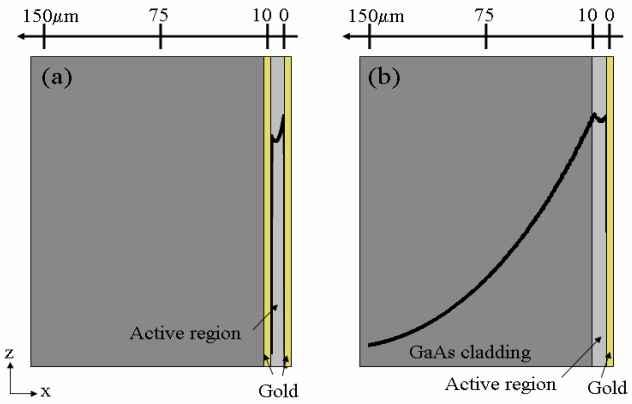

Fig. 1. Schematic representation of (a) double- and (b) single-metal THz QCL waveguides. The component of the magnetic field of the mode parallel to the layers of the active region (H_y) is plotted.

The focus of this work is to implement surface emission via a second-order grating in a double-metal waveguide THz QCL. Double-metal waveguide THz QCL devices have much better mode confinement and temperature performance than single-metal waveguide devices, making them a more favorable technology for THz QCLs. In addition, surface-emitting double-metal THz waveguides can be used in future THz sources that use difference-frequency generation between two mid-infrared laser modes. Here, the dielectric waveguide containing the active region for dual wavelength mid-infrared QCLs with integrated optical nonlinearity may be placed between two metal claddings to provide a good waveguide for the THz difference-frequency mode.

The paper is organized as follows: in the second section, the optimal second-order grating design is calculated for surface emission in a double-metal waveguide QCL operating at approximately 3THz. The third section then covers the details of the device fabrication and presents the experimental results of this study.

2. Theory

The mechanism for surface emission via a second-order grating is described with distributed feedback (DFB) grating theory. DFB structures do not utilize conventional cavity mirrors for feedback, but rather periodic perturbations of the refractive index [11] that support Bragg scattering. Consider the lasing mode to be decomposed into right- and left-propagating waves in the laser cavity; feedback occurs when the counter propagating waves scattered from the grating constructively interfere for some scattering diffraction order. For a second-order diffraction grating, first-order diffraction is perpendicular to the plane and contributes to surface emission, and second-order diffraction is in-plane with the cavity and provides feedback [12].

To quantify the feedback and surface emission in double-metal waveguides, we use the formalism described in [13]. First, we use Comsol Multiphysics software to solve for the eigenmodes of an infinitely long laser cavity using a single grating unit cell with periodic boundary conditions. We then compute the coupling constant κ using these eigenmodes and use κ in the coupled mode equations that describe dynamics in a finite-length structure [13]. The analyzed double metal structure is presented in Fig. 2(a). Figures 3(a) and 3(b) show the two relevant modes for this structure; one mode [Fig. 3(a)] is symmetric with respect to the grating in the unit cell and contributes to surface emission, while the other mode [Fig. 3(b)] is anti-symmetric with respect to the grating and does not contribute to surface emission.

#75601 - $15.00 USD Received 29 September 2006; revised 26 October 2006; accepted 9 November 2006

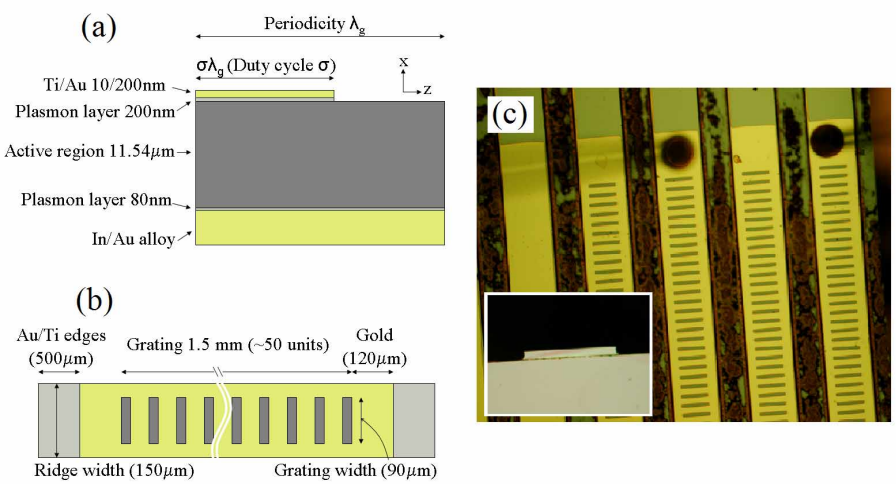

Fig. 2. Schematics of the surface emitting THz QCL design: (a) side view and (b) top view. The side view shows one grating unit. (c) Optical microscope image of the processed devices: top and side view (inset) of the ridges.

In classical distributed feedback theory, the boundaries are considered perfectly anti-reflecting and feedback is due entirely to Bragg scattering from the grating [11]. With these boundary conditions, the coupled mode equations can be solved for the frequencies, amplitudes, and relative phases for the left- and right-propagating waves of a DFB mode *i*, with envelope functions $S_i(z)$ and $R_i(z)$, respectively [11-13]. The second-order grating creates a gap in the frequency spectrum of the modes. The two modes with the lowest threshold gain are those on each side of the gap [11,12]. The phase relationships between left- and right-propagating waves for these two modes are such that for one of the modes (the "symmetric" mode), surface emission from left- and right-propagating waves interferes constructively, while for the other mode (the "anti-symmetric" mode) the interference is destructive [12]. The anti-symmetric mode thus has a lower threshold gain because of the greatly reduced surface-emission losses and becomes the lasing mode [12,13]. This mode still provides surface emission, however, because $S_i(z)$ and $R_i(z)$ differ in magnitude near the device edges since the anti-reflecting boundary conditions make $S_i(z)$ and $R_i(z)$ zero at the right (left) edges of the device [12-14].

It is possible to obtain surface emission with the second-order grating for a device with partially or fully reflecting boundary conditions. However, in this case, the lasing mode strongly depends on the placement of reflective facets relative to the grating, due to the interference of left- and right-propagating waves with the reflected waves at the boundaries [16-17]. Reference [15] suggests that for THz resonators, the facets can be fabricated with sufficient precision relative to the grating to enforce the lasing in the symmetric mode. However, facets with high reflectivity will also provide feedback for low-loss, poor surface-emitting higher-order lateral modes. With low surface-emission losses, these modes will be preferred for lasing. Note that one can suppress the higher-order lateral modes by making THz QCLs with narrow (20-50μm wide) ridges [6]. However, in this case, the surface-emission divergence in the direction perpendicular to the ridge becomes high. We choose to suppress the Fabry-Perot feedback in our devices so that only DFB modes supported by the second-order grating exist in the laser cavity.

For double-metal waveguides, facet reflectivity has been calculated to be as high as 80-90% at 3 THz [6]. To suppress the reflectivity, we fabricate devices with "absorbing edges", see Fig. 2(b). The absorbing edges are the sections of the double-metal waveguide in which titanium alone is used for the top metal cladding instead of titanium and gold. This increases waveguide losses from approximately 20 cm^{-1} to approximately 300 cm^{-1}. We use 500μm-

#75601 - $15.00 USD Received 29 September 2006; revised 26 October 2006; accepted 9 November 2006

long absorbing edges for both facets; this is sufficient to completely suppress the reflections from the waveguide facets. We estimate using Finite Difference Time Domain (FDTD) calculations that the reflectivity at the interface between the grating section and the absorbing edges is less than 5%.

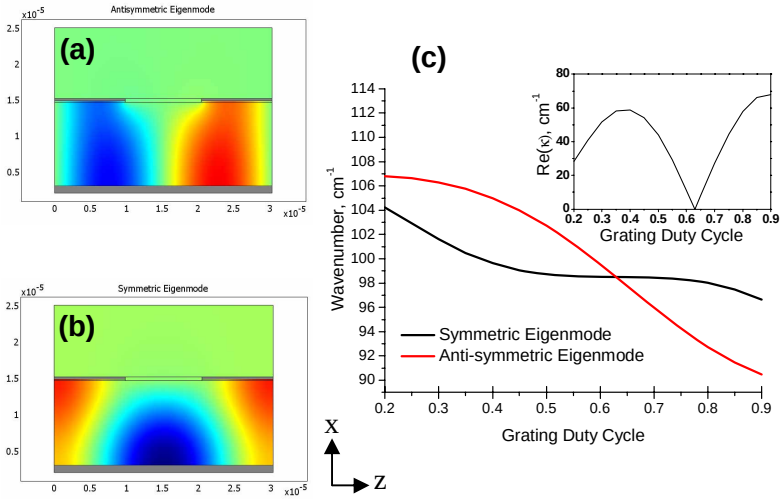

Fig. 3. Antisymmetric (a) and symmetric (b) eigenmode profiles (H_y component) for the infinite grating structure. The gold cladding is colored in gray. (c) Eigenmode frequency (in wavenumbers) as a function of the grating duty cycle for a grating structure with a periodicity of 30.4μm. Inset: Real part of the coupling constant calculated using Eq. (1).

The efficiency of surface emission and the threshold gain for DFB modes depends strongly on the grating periodicity and duty cycle. The grating periodicity must be adjusted so that the energies of the lowest threshold gain DFB modes coincide with the peak of the QCL gain [14]. The choice of the grating duty cycle is determined by the optimal value of the coupling constant κ. For efficient surface emission, the second-order grating must provide a coupling constant such that $|\kappa|L \sim 1-2$, where L is the length of the cavity [14]. For THz double-metal surface-plasmon waveguides, the metal gratings interact strongly with the laser mode, generally resulting in $|\kappa|L >> 1$ for typical device lengths of 1-3mm [15]. However, it is pointed out in Ref. [15] that there exists a narrow range of grating duty cycles where the coupling constant is significantly reduced. To calculate κ, we use the expression from Ref. [13],

$$\kappa = \frac{(k_s - k_{as})k_g}{2k_0} + \frac{\alpha_s^{surf} + \alpha_s^{wg} - \alpha_{as}^{wg}}{2} i \qquad (1)$$

where $k_g = 2\pi/\lambda_g$ is the grating wavevector with λ_g being the grating period, k_0 is the free space wavevector corresponding to the lasing frequency, α_s^{surf} is the surface-emission loss for the symmetric eigenmode calculated for the infinite grating, and α_s^{wg} (α_{as}^{wg}) and k_s (k_{as}) are the waveguide losses and the free space wavevector, respectively, for the symmetric (anti-symmetric) eigenmode calculated for the infinite grating structure. As shown in Ref. [15], the imaginary part of κ is much smaller than its real part for most values of the grating duty cycle and is slowly varying as a function of the grating duty cycle. We use Comsol Multiphysics to calculate the values of k_s and k_{as} for the infinite grating structures, shown in Fig. 2(a), with different grating duty cycles. The results of the calculations for a 30.4μm grating are shown in Fig. 3(c) along with the corresponding values of $\mathrm{Re}\{\kappa\}$ obtained using Eq. (1). One can see from Fig. 3(c) that $\mathrm{Re}\{\kappa\} = 0$ for a grating duty cycle of

#75601 - $15.00 USD Received 29 September 2006; revised 26 October 2006; accepted 9 November 2006

0.63. Theoretically, a grating with exactly this periodicity will be purely loss-coupled. In practice, gratings should not be designed with the duty cycle at which $\mathrm{Re}\{\kappa\}=0$ because total cavity losses become extremely high [15]. A more realistic grating design is one slightly off-resonance from the crossover point. We chose to fabricate the structure with a grating duty cycle of 0.65 and estimate $\mathrm{Re}\{\kappa\}$ to be ~8 cm^{-1} for this duty cycle.

We note that all the data shown in Fig. 3 is obtained for two-dimensional ("infinite width") structures. The actual structure of the device [Fig. 2(b)] has a grating that spans only a fraction of the lateral width of the ridge, meaning that only a fraction of the waveguide mode overlaps with the grating. The rest of the mode overlaps with a double metal section of the waveguide, which provides sufficient conductivity for the top of the ridge to function as a proper electrical contact. This also leads to a shift in eigenmode frequency and to smaller values of $\mathrm{Re}\{\kappa\}$ for the actual device than that estimated theoretically. To accommodate for these differences as well as for the inaccuracies of the theoretical calculations, we fabricate devices with different grating periods. Devices with different grating duty cycles will be the subject of future studies.

3. Fabrication and experimental results

Double-metal waveguide THz QCLs were processed from a GaAs-AlGaAs heterostructure based on the bound-to-continuum design reported in Ref. [18]. The heterostructure was grown by molecular beam epitaxy on a semi-insulating GaAs substrate; the growth started with a 200nm-thick $Al_{0.5}Ga_{0.5}As$ etch-stop layer on an undoped GaAs buffer layer and was followed with a 200nm thick n = 2×10^{18} cm^{-3} GaAs plasmon layer and 90 periods of the active region, totaling 11.57μm. The growth ended with a GaAs plasmon layer 80nm thick doped at n = 5×10^{18} cm^{-3}. Double-metal waveguide fabrication follows Ref. [4] closely. Figures 2(a) and 2(b) display all relevant dimensions for the surface-emitting device. For processing, one square centimeter of QCL material is cleaved and Ti/Au (10nm/900nm) is deposited by electron-beam evaporation. The wafer is bonded at 250 degrees Celsius to a highly doped GaAs substrate with deposited layers of Ti/Au/In (20nm/75nm/1400nm). The bonded QCL wafer is then lapped down and wet etched to the etch-stop layer with a hydrogen peroxide and sodium hydroxide solution (19:1 in volume), and the etch stop layer is stripped with hydrofluoric acid. The laser ridge is defined by a dry etch, utilizing a Cl_2 and BCl_3 mixture and a mask comprising SU-8 photoresist (Microchem) on top of a thin layer of Omnicoat (Microchem). After etching, SU-8 is stripped off in PG Remover (Microchem). Next, top contacts (Ti/Au, 10nm/200nm) with gratings are defined on top of the ridges by a liftoff procedure. Subsequently, 200nm of the highly doped plasmon layer is removed beneath the grating openings by dry etch with a Cl_2 and BCl_3 mixture, where the gold is used as a self-aligned mask. To define absorbing edges at both edge facets for surface-emitting devices, gold is removed from the ends of the QCL waveguides using optical lithography and gold wet etching (Transene Gold Etch); the sticking layer of 10nm of Ti beneath the gold is not removed. Two 120μm-long sections of gold near each of the absorbing edges are left for bonding. The wafers are then polished down to a thickness of 200 microns, and Ti/Au (20nm/200nm) is deposited on the back side of the substrates. Devices are cleaved into 2.74mm bars, mounted on a copper mounting block, and placed in a helium-flow cryostat. Figure 2(c) displays optical microscopy images of the processed and bonded devices.

#75601 - $15.00 USD Received 29 September 2006; revised 26 October 2006; accepted 9 November 2006

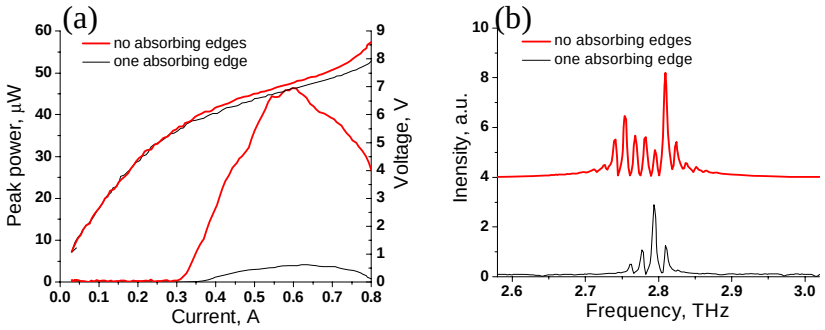

Fig. 4. L-I and I-V (a) and spectra (b) for Fabry-Perot structures with and without an absorbing edge at 5K.

To characterize the lasing material and absorbing edge concept, normal double-metal structures and double-metal structures with a 0.5mm-long absorbing edge on one side are tested in an edge emitting configuration. Devices are tested in pulsed mode with 100ns pulses at a 200 kHz repetition rate. Peak powers are measured with a calibrated helium-cooled bolometer using two 2" diameter parabolic mirrors: one with a 5 cm focal length to collect light from the device and the other with a 10 cm focal length to refocus it to the detector. For the device with an absorbing edge, radiation is collected from the end without the titanium absorber. Figure 4(a) displays L-I and I-V characteristics for a 2.74mm-long double-metal waveguide THz QCL with and without an absorbing edge. Figure 4(b) shows the spectra of the devices, which contains many Fabry-Perot modes. For the device without absorbing edges, the mode spacing is measured to be 14.1 GHz (0.47 cm^{-1}), which corresponds to a mode index of refraction of 3.7 given the device length. The threshold current density is 73A/cm^2, the collected peak power at 5K is 38 μW, and the maximum device operating temperature is 85K. For a device with the absorbing edge, threshold current density at 5K is approximately 87 A/cm^2, the collected peak power at 5K is 4 μW, and the maximum device operating temperature is 75K. Mode spacing for this device [Fig. 4(b)] is measured to be 16.5 GHz (0.55 cm^{-1}), which yields a device length of 2.34 mm given a mode refractive index of 3.7. This value is similar to the total length of the gold-coated section of the ridge (2.24 mm) and indicates that feedback for lasing comes from reflection at the boundary of the double metal waveguide and the absorbing edge. Thus, the absorbing edge reduces facet reflectivity, but further improvement in absorbing edge design will be necessary in the future.

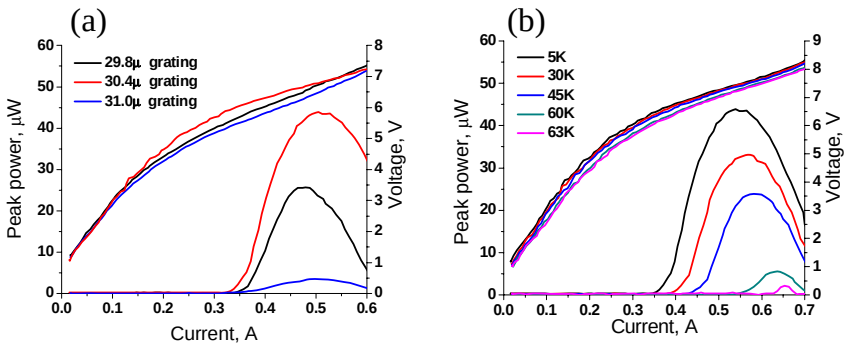

Fig. 5. (a). L-I and I-V characteristics at 5K of surface-emitting devices with a 1.5mm-long grating section, a grating duty cycle of 0.65, and different grating periodicities. (b) L-I and I-V characteristics at different temperatures for a surface-emitting device with a 30.4μm grating.

Figure 5(a) shows L-I and I-V characteristics of surface-emitting devices with different second-order grating periodicities at 5K. Radiation is collected with the parabolic mirror setup described above and the bolometer has a built-in Winston cone with a 2 cm wide aperture. This ensures the collection of surface-emitted radiation emitted from the whole

#75601 - $15.00 USD Received 29 September 2006; revised 26 October 2006; accepted 9 November 2006

grating length. The grating duty cycle for all devices is approximately 0.65. The peak powers at 5K from devices with 29.8 μm, 30.4 μm, and 31.0 μm gratings are 26 μW, 39 μW, and 4 μW respectively. Figure 5(b) shows L-I and I-V data for a device with 30.4μm grating at different temperatures. The peak power is measured at 5K for this device and is similar to the peak power measured from the 2.74mm-long edge-emitting Fabry-Perot device. The maximum operating temperature for the 30.4 μm grating device is 63K and the threshold current density at 5K is approximately 100 A/cm^2. The maximum operating temperature is lower and the threshold current density is higher for the surface emission device in comparison with the edge emitting device. This is expected due to increased loss and reduced confinement in the waveguide for the surface emitting device. However, the slope efficiency of the 30.4μm grating device is approximately a factor of two higher than that of the edge-emitting Fabry-Perot device, see Figs. 4(a) and 5(a). This indicates that THz outcoupling is more efficient for a 30.4μm grating surface-emitting device than for an edge-emitting device.

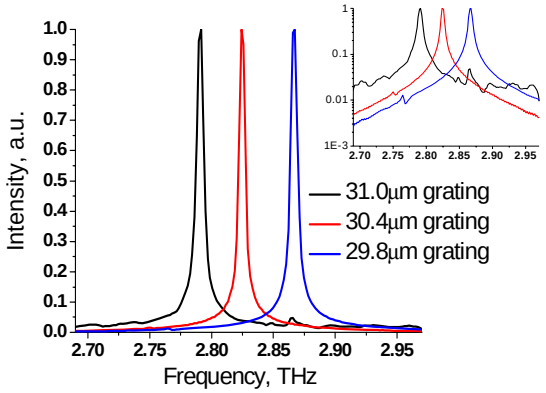

Fig. 6. Spectra from 1.5mm long surface-emitting devices operated in pulsed mode at T=5K. Spectra are normalized to unity.

Figure 6 displays the spectra for the surface-emitting devices with grating periods of 29.8 μm, 30.4 μm, and 31.0 μm operating at 5K in pulsed mode. The spectral peaks for the devices are at 2.790 THz, 2.825 THz, and 2.865 THz, respectively. For the devices with 30.4μm and 31.0 μm gratings, the emission spectra are single mode with a side mode suppression ratio of more than 20 dB. The surface-emission frequency generally agrees with theoretical predictions.

For the 30.4μm grating device, the three-dimensional DFB mode has a calculated effective refractive index of 3.49 that yields a lasing frequency at 2.83 THz, close to the measured value of 2.825 THz. Here, we assume an active region refractive index that yields a mode effective refractive index of 3.7 for a two-dimensional double-metal waveguide. Similarly, the DFB mode frequencies for devices with 29.8 μm and 31.0 μm gratings are calculated to be at 2.85 THz and 2.80 THz respectively, which are close to the measured values.

The hallmark for surface emitting lasers is highly directional emission, and the far-field profile along the laser ridge for a device with a 30.4 μm grating is shown in Fig. 7. The full-width half-maximum (FWHM) of the far-field lobe is measured to be 6 degrees. A double-lobed profile is typically expected for a surface-emitting device with a second-order grating [13]. This is not observed most likely due to the insufficient angular resolution of our setup. In addition, finite reflectivity at the laser and absorbing edge boundary may affect the surface emission far-field profile [12].

We note that, while the directionality of the emission along the laser ridge is determined by the length of the second-order grating, the directionality of the emission perpendicular to the ridge is determined by the grating width. For the devices discussed here, the grating width is 90 μm, which is smaller than the wavelength of emitted THz radiation in air, $\lambda \approx 106$ μm.

#75601 - $15.00 USD Received 29 September 2006; revised 26 October 2006; accepted 9 November 2006

Therefore, these devices still have high far-field divergence in the direction perpendicular to the ridge. We have measured the far field in the direction perpendicular to the ridge within ±20 degrees from the normal to the grating surface (limited by our setup) and did not observe clear directionality. To improve directionality of the THz output in the direction perpendicular to the ridge, one can process devices with wider ridges and gratings, cf. Ref. [9]. Making surface-emitting THz QCLs with wider gratings, along with the investigation of other designs, will be part of our future work in improving efficiency and directionality of surface-emission in THz QCLs with double-metal waveguides.

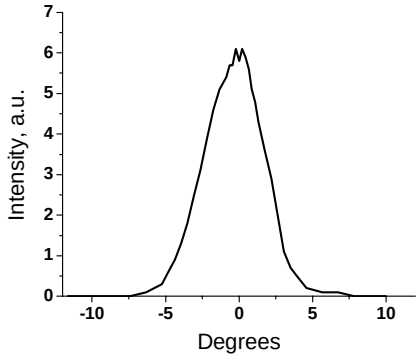

Fig. 7. Far-field profile along the ridge (z-axis) of a 30.4μ surface-emitting structure operated in pulsed mode at T=5K. The FWHM is approximately 6 degrees.

4. Conclusions

We have demonstrated surface emission in double-metal waveguide THz QCLs by using a second-order metal grating. Conventional DFB theory requires the facets of the laser cavity to be anti-reflecting, so that the feedback in the cavity is due only to Bragg reflections. Finite facet reflectivity may spoil surface emission by allowing the device to incorporate Fabry-Perot feedback and support low-loss, poor surface emitting lasing modes. To incorporate anti-reflecting boundary conditions in double-metal waveguides, we fabricate absorbing Ti-Au sections at the ends of the Au-Au waveguide. The surface emission efficiency is optimized by calculating a regime of grating duty cycles that minimizes the coupling constant κ. The result is working devices that are single mode and that have output powers approximately as high as those from reference edge emitting devices. The slope efficiencies of the surface-emitting devices are measured to be twice that of the edge-emitting devices. The far-field profile of the surface-emitting devices is highly directional along the laser ridge.

Acknowledgments

This work was supported by AFOSR under Contract No. FA9550-05-1-0435 (Gernot Pomrenke). The structures were processed in the Center for Nanoscale Science (CNS) in Harvard University. Harvard-CNS is a member of the National Nanotechnology Infrastructure Network. Material growth was supported by EPSRC (UK). J.F. acknowledges support from the NSF Graduate Fellowship. S.K. acknowledges support from HMGCC.

#75601 - $15.00 USD Received 29 September 2006; revised 26 October 2006; accepted 9 November 2006